

Ordered Vacancy Network Induced by the Growth of Epitaxial Graphene on Pt(111)

G. Otero,¹ C. González,¹ A. L. Pinaridi,¹ P. Merino,² S. Gardonio,^{3,*} S. Lizzit,³ M. Blanco-Rey,⁴ K. Van de Ruit,⁵
C. F. J. Flipse,⁵ J. Méndez,¹ P. L. de Andrés,¹ and J. A. Martín-Gago^{1,2}

¹*Instituto Ciencia de Materiales de Madrid (CSIC), C. Sor Juana Inés de la Cruz 3, 28049-Madrid, Spain*

²*Centro de Astrobiología, INTA-CSIC, Torrejón de Ardoz, 28850 Madrid, Spain*

³*Sincrotrone Trieste SCpA, Strada Statale 14, Km. 163.5, 34149 Trieste, Italy*

⁴*Department of Chemistry, University of Cambridge, Cambridge CB2 1EW, United Kingdom*

⁵*Department of Applied Physics, Eindhoven University of Technology, P.O. box 513, 5600 MB Eindhoven, The Netherlands*

(Received 14 July 2010; revised manuscript received 23 September 2010; published 19 November 2010)

We have studied large areas of $(\sqrt{3} \times \sqrt{3})R30^\circ$ graphene commensurate with a Pt(111) substrate. A combination of experimental techniques with *ab initio* density functional theory indicates that this structure is related to a reconstruction at the Pt surface, consisting of an ordered vacancy network formed in the outermost Pt layer and a graphene layer covalently bound to the Pt substrate. The formation of this reconstruction is enhanced if low temperatures and polycyclic aromatic hydrocarbons are used as molecular precursors for epitaxial growth of the graphene layers.

DOI: 10.1103/PhysRevLett.105.216102

PACS numbers: 68.35.-p, 68.37.Ef, 68.43.Fg, 68.65.Pq

Recent experiments on epitaxial graphene layers grown on metal surfaces have raised hopes of developing a large number of applications [1,2]. Therefore, understanding the growth, morphology, and structure of these layers is an active research subject owing to its fundamental and practical interest. Graphene layers can be efficiently grown by thermal decomposition of small organic molecules, usually ethylene, on transition metals, such as Ru(0001) [3,4], Ir(111) [5], Rh(111) [6], and Pt(111) [7,8]. The morphology and structure of the graphene layer are intensively discussed in the literature, and the strength and nature of the interaction of the layer with the metal substrate is still under debate. The formation of nanometric size graphene in the form of islands, patches, or defective areas with the supporting metallic substrate could give rise to tailored electronic properties, as it has been recently reported [9–11]. This interaction is directly related to the distance between the metal surface and the graphene layer, and determines, for instance, the amount of rippling for Moiré patterns. Earlier theoretical models have used a simple parametrized tight-binding approach relying on a weak interaction (large separation) between both systems, while other models based in *ab initio* approaches have argued in favor of shorter distances and a stronger interaction (e.g., [4]).

Typical for graphene on transition metal surfaces is the development of Moiré patterns exhibiting large surface unit supercells with periodicities of about 2–3 nm. Ru and Ir surfaces develop extended single-domain graphene layers, as depicted by scanning tunneling microscopy (STM) images [3,5]. Pt, on the contrary, shows incommensurate domains coexisting with Moiré patterns of different periodicities on the same surface [7,8]. In this work we focus on the formation and structure of previously reported graphene regions, which are commensurate with a Pt(111)

substrate in small crystallographic ratios, i.e., forming a $(\sqrt{3} \times \sqrt{3})R30^\circ$ periodicity [7]. We will show that this structure is the result of a large surface-overlayer interaction that accommodates its large mismatch by inducing a strong reconstruction on the Pt surface. These regions, presenting smaller crystallographic ratios than the Moiré counterpart, make the system amenable to be explored by *ab initio* calculations, an important tool to accurately interpret the chemistry and physics of epitaxial graphene [4,11,12]. Therefore, this system offers a unique opportunity to test theories and structural parameters that are relevant to understand the interaction of graphene with transition metal surfaces.

Wide $(\sqrt{3} \times \sqrt{3})R30^\circ$ areas are formed by slowly evaporating (up to 1 h) in ultrahigh vacuum conditions the equivalent coverage of 3 ML of molecular precursor on an atomically clean Pt(111) surface at 900–1000 K ($P < 7 \times 10^{-10}$ mbar). The substrate temperature is chosen as the minimum temperature for molecular decomposition. We have found that low formation temperatures (900–1000 K) and the use of large polycyclic aromatic precursors, such as $C_{60}H_{30}$ [13] or C_{60} fullerenes, instead of the standard ethylene, strongly favor the amount of the $(\sqrt{3} \times \sqrt{3})R30^\circ$ areas with respect to Moiré structures. See the supplementary material [14] for more details. Using these preparation conditions, large scan STM images show that about 15%–20% of the sample is covered with islands exhibiting this reconstruction. Although the relative ratio of the $(\sqrt{3} \times \sqrt{3})R30^\circ$ areas with respect to the Moiré structures changes upon experimental conditions, the periodicities of the structures formed are always the same. Low-energy electron diffraction patterns and the attenuation of the x-ray photoelectron spectroscopy (XPS) signal suggest that a single carbon layer remains on the surface, in good agreement with previous studies [6]. STM images

were acquired both at room temperature and at 77 K, and the use of different tunneling parameters shows in all cases images with similar atomic features.

At or above the monolayer coverage, the $(\sqrt{3} \times \sqrt{3})R30^\circ$ areas could extend to the whole Pt-terrace length (up to 100 nm) as shown in Figs. 1(a) and 1(b). Figure 1(a) corresponds to a wide-scan topographic STM image obtained at submonolayer graphene coverage where clean Pt terraces coexist with Moiré patterns and $(\sqrt{3} \times \sqrt{3})R30^\circ$ regions. Each of these regions has been identified by high magnification images on the labeled areas. On the Moiré regions, we observe the recently reported nanobubbles [9]. Each domain shows long-range order convincingly. The $(\sqrt{3} \times \sqrt{3})R30^\circ$ phase coexists with Moiré regions of different periodicities [see Fig. 1(b)], and it has never been found isolated [7,8]. Figure 1(c) shows a detailed STM image where the atomic features forming the $(\sqrt{3} \times \sqrt{3})R30^\circ$ reconstruction are clearly identified. These images are characterized by bright points and depressions aligned along the $[1\ 1\ \bar{2}]$ surface crystallographic direction. This structure exhibits large atomic corrugation in the STM images, ranging from 0.60 to 0.15 Å, about 5 times higher than those we have obtained for the corresponding Moiré regions under the same conditions (< 0.1 Å) [3]. Since electronic effects are important in the image appearance, the atomic assignment of the STM features shown in Fig. 1(c) is not trivial and requires the use of first-principles calculations.

We have used *ab initio* density functional theory (DFT) to locate the equilibrium ground state of the system by searching for a total energy global minimum. Wave functions are expanded in plane waves up to a cutoff of 350 eV and are sampled on a Monkhorst-Pack $6 \times 6 \times 1$ mesh inside the Brillouin zone (see Ref. [14] for more details). C and Pt atoms are described by ultrasoft pseudopotentials, and the local density approximation is used for exchange

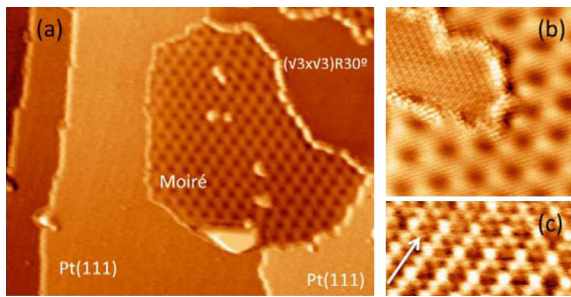


FIG. 1 (color online). Constant-current STM images showing islands with the $(\sqrt{3} \times \sqrt{3})R30^\circ$ structure. Scanned area of panels are (a) 52×41 nm², (b) 12×12 nm², and (c) 3.2×1.3 nm². Bias voltages range from 20 to 100 mV and tunnel currents from 0.1 to 4 nA. The arrow indicates the $[1\ 1\ \bar{2}]$ surface direction. The image (a) was recorded for a partially covered surface, where the growth process was stopped before saturation. Panels (a) and (b) show the $(\sqrt{3} \times \sqrt{3})R30^\circ$ superstructure coexisting with a Moiré region.

and correlation. DFT calculations are performed with the CASTEP code [15]. This formalism yields lattice parameters for bulk fcc platinum of 2.774 Å (fractional error -0.05%) and for an isolated graphene layer of 2.440 Å (fractional error -0.87%). The clean Pt(111) surface shows an outwards relaxation of $+1.0\%$ and a second layer contraction of -0.2% , in good agreement with previous experimental determinations ($+0.8\%$ and 0.0%).

A 30° rotation between the Pt and C structures reduces the mismatch between Pt and graphene meshes from 11% to about 3%. Such a mismatch, however, is still large and elastic distortions in the graphene layer result in an increase of the total energy, which can be interpreted as an effective repulsive interaction between graphene and platinum. Under these conditions the graphene layer stays at a relatively large distance from the outermost Pt(111) layer (3.31 Å), remaining atomically flat with very little buckling ($z = 0.01$ Å). These values are similar to those calculated for the low-interacting Moiré regions [3,12], and in contrast to large atomic corrugation measured in the STM images [Fig. 1(c)].

A different way to release stress is to induce a reconstruction on the Pt(111) surface. We have found that the formation of an ordered network of Pt vacancies at the outermost layer leads to an energetically stable structure compatible with the STM images. After trying many different structures (including lateral shifts in the graphene layer, extra carbon atoms, and vacancies in both layer and surface), our best-fit model is depicted in Fig. 2. In this model one surface Pt atom is missing per $(\sqrt{3} \times \sqrt{3})R30^\circ$ unit cell, and the rest of the Pt atoms are alternatively in top or hollow positions with respect to the graphene layer. DFT calculations show that graphene binds more strongly to the platinum surface in the presence of vacancies. The interaction becomes 3 times larger (-0.60 eV per unit cell), and the bond length between the C near a top Pt shortens to 2.28 Å (see Fig. 2, side view). The remaining seven C atoms in the unit cell relax outwards, producing a maximum buckling in the C layer of $\Delta z = 0.2$ Å. This number is about 7 times smaller than the one quoted for long-range ripples in graphene [11]. The outermost Pt layer goes from expansion to -8.1% contraction.

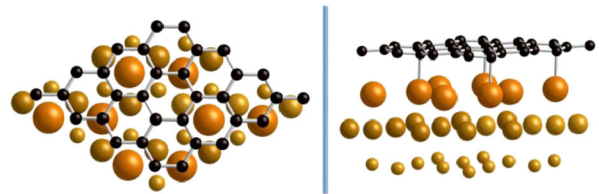


FIG. 2 (color online). Top view (left) and side view (right) of the structural model derived from DFT calculations for the $(\sqrt{3} \times \sqrt{3})R30^\circ$ reconstruction. Smaller sizes on the spheres represent deeper atoms. The side view is slightly tilted for a better visualization of the vacancy channels and interaction between C (black) and surface Pt [gray (yellow)] atoms.

To accurately relate this structural model with the experimental STM images we have performed theoretical simulations using a non-equilibrium Keldysh Green function formalism in which multiple scattering events have been considered. The FIREBALL program has been used to compute a DFT Hamiltonian based on a linear combination of orbitals [16]. A tip made with 105 tungsten atoms forming a pyramidal cluster ending in a single atom on a W(100) terrace has been used. STM simulations have been performed on the structural model previously optimized using the more accurate plane-waves formalism. Figure 3 compares the calculated STM image with a high-resolution experimental one. Important features observed in our experiments, i.e., the bright spots and the depressions surrounded by a tiny halo, are very well reproduced in our simulations, and even quantitative agreement can be seen in the scan lines (see Ref. [14] for details). The total corrugation of the theoretical model for different tip distances range from 0.1 to 0.3 Å, in good agreement with the experimental values. Although C atoms are more than 2 Å above the outermost Pt layer, it is important to notice that the STM image essentially reflects the Pt atoms because of the large difference in the density of states (DOS) contribution around the Fermi level. Additionally, the tip-surface distance has been reduced more than 1 Å with respect to the Moiré regions, increasing the Pt-tip hopping by a factor of 16, which prevents the measurement of atomic corrugation from the C atoms in the STM images of the $(\sqrt{3} \times \sqrt{3})R30^\circ$ superstructure [16]. The calculation shows the Pt on hollow positions presents the strongest contribution, appearing as the brightest in the image. Finally, the C atoms from the graphene layer produce multiple scattering processes in the tunneling current, which are responsible for the tiny circular features observed in the STM images around the Pt vacancies that have a C on top [Fig. 3].

This atomic model agrees very well with STM images, and it is also supported by high-resolution x-ray photoelectron spectroscopy (XPS) data recorded in the SuperESCA beam line of the synchrotron radiation facility Elettra. Figure 4 shows the C 1s core level spectra of graphene prepared by ethylene dissociation following the standard recipe described in Refs. [3,4,6] (upper spectrum), and the one grown using C₆₀ as molecular precursors (lower spectrum). In the latter case the STM images

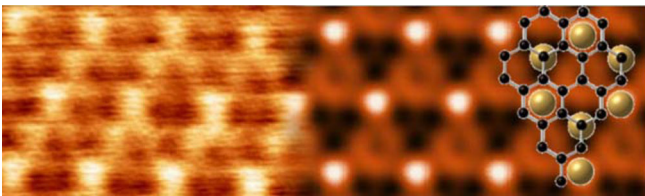


FIG. 3 (color online). STM image ($V = 0.1$ V) for the $(\sqrt{3} \times \sqrt{3})R30^\circ$ experimental (left) and DFT best-fit simulation (right). A schematic atomic model has been overlaid. Both images are merged in the central part.

show the coexistence of several phases, including the $(\sqrt{3} \times \sqrt{3})R30^\circ$ reconstruction. The peak corresponding to the ethylene preparation shows a single component centered at 284.0 eV, whereas the lower peak corresponding to graphene grown with C₆₀ shows extra components at both sides of the main peak (284.3 and 283.7 eV). Thus, the main peak corresponds to the low-interacting Moiré regions, and its binding energy is in agreement with previously published results [6]. The small components can be related to the existence of the covalently bonded structures. It has been shown that the core level peak of C atoms interacting with transition metal substrate is shifted towards higher binding energies [6,17]. In the model proposed in Fig. 2 for the $(\sqrt{3} \times \sqrt{3})R30^\circ$ phase there are three different types of C atoms: over a Pt vacancy, on top of a surface Pt, and in bridge position. These three C atoms present different total charges, as depicted by CASTEP calculations: $-4.08e^-$, $-4.15e^-$, and $-4.08e^-$, respectively. We expect this charge redistribution, including final state effects, to be reflected in the final binding energy of the C 1s core level peak, similar to the example shown in Ref. [17]. Moreover, a XPS calculation of the areas involved in the different structures gives a value of about 21% of the sample covered with these covalently bound phases, in good agreement with the STM observation of 15%–20% for these experimental conditions.

In this structural model, graphene forms new bonds with Pt atoms as it has been observed by analyzing the charge density difference for the optimum configuration displayed in Fig. 2: C p_z orbitals interact with Pt dz^2 ones accumulating charge in the intermediate region. The main effect of vacancies on the Pt electronic structure is a subtle one: the d band narrows and moves down in energy towards the Fermi energy by about 0.3 eV. Therefore, the center of mass for the Pt d band gets closer to the C π band, increasing hybridization and chemical interaction. From the point of view of the electronic structure of carbon

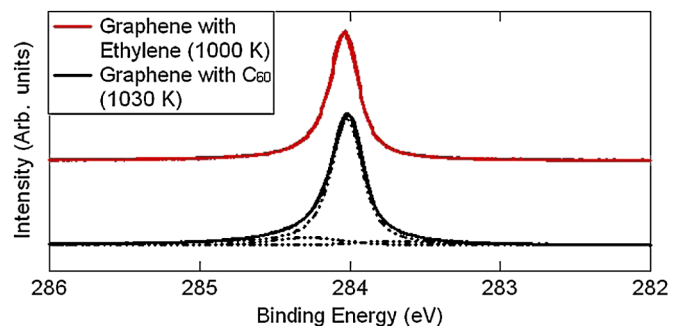


FIG. 4 (color online). C 1s core level spectra of graphene grown on Pt(111) recorded with 400 eV of photon energy. Upper spectrum using ethylene decomposition (red line), lower spectrum using polycyclic molecular precursors and experimental conditions in which the $(\sqrt{3} \times \sqrt{3})R30^\circ$ phase coexists with Moiré regions on the surface (black line). Dashed lines correspond to the best-fit components.

atoms the main change is an important increase in the DOS at the Fermi level for π bands, which could enhance the local catalytic properties of these reconstructed regions.

At first glance, the proposed Pt surface reconstruction might be thought unlikely since it involves kinetic barriers larger than 3 eV. However, the existence of a network of vacancies after deposition and decomposition of large organic molecules is widely supported by different experimental observations. First, it has been shown that a graphene layer interacting with the substrate via weak van der Waals forces tends to form ripples with large spatial periodicities [18]. However, the $(\sqrt{3} \times \sqrt{3})R30^\circ$ regions shown in Fig. 1 do not show ripples, but a large atomic corrugation (more than 5 times larger than the Moiré regions). This suggests that covalent bonds have been formed between the layer and the substrate. Second, STM images for clean Pt(111) show typical large terraces separated by steps running parallel to the surface crystallographic directions. STM experiments for graphene on Ru (0001) and Ir(111) show that steps remain sharp and adjusted to surface crystallographic directions after the graphene layer has been created [3,5]. In our case, however, when the $(\sqrt{3} \times \sqrt{3})R30^\circ$ phase is on the surface, we observe a rounding of the surface steps, as can be seen in Fig. 1(a) for an incomplete coverage. Steps separating Pt terraces are straight, whereas the ones separating graphene regions are curved. See the supplementary material [14] for more STM images showing this effect. The step smoothing process has been observed for different graphene overlayers. For instance, in the case of the $(\sqrt{19} \times \sqrt{19})R23.4^\circ$ formed after decomposition of benzene at high temperature, a reorganization of the last Pt layer has been suggested [8]. Rounding of steps is usually associated with transport of Pt atoms from the terraces, and we introduce the following model to explain this experimental evidence: upon annealing the molecular precursor, a Pt atom per $(\sqrt{3} \times \sqrt{3})R30^\circ$ unit cell is removed from the surface and diffuses towards the step edges, leaving a vacancy behind [8,19]. The energy necessary to overcome the large kinetic barrier should be found in the complex reorganization of the large carbon-based precursors. Indeed, it has been reported in the literature that annealing at lower temperatures of different organic molecules, such as fullerenes, results in the ejection of Pt atoms out of the surface, creating vacancies on the Pt surface layer [19]. The same mechanism has been proposed for C_{60} on Pd (110) [20], and more recently for Ag(111) [21] and Pt(110) [22]. In these cases, the C_{60} adsorbs with a hexagon on the vacancy maximizing the number of C-Pt bonds. However, in our case, the orientation of the C layer with respect to the substrate is imposed by minimization of the stress between

both structures resulting in a C atom placed on top of the vacancy. Furthermore, the clean Pt(111) surface is known to show a tendency to reconstruct at high temperatures [23]. The organic polycyclic molecules used as precursors get enough energy to facilitate the breaking of strong C-C bonds and decompose once in contact with the reactive surface Pt atoms. The adsorption, bond breaking, and interaction of carbon species modifies the energetic balance resulting in the formation of new binding forces, inducing the formation of vacancies. Thus we conclude that the mechanism of vacancy formation in Pt(111) upon annealing is likely when large carbonaceous species interact with the Pt surface, as it has also been reported for other transition metals.

We acknowledge financial support from the Spanish projects MAT2008-1497 and CSD2007-41. C.G. and P.M. acknowledge financial support by the CSIC JAE-Doc contract and from the INTA program ‘‘Rafael Calvo Rodés,’’ respectively. We acknowledge funding from the European Community’s Seventh Framework Program (FP7/2007-2013) under Grant Agreement No. 226716.

*Permanent address: University of Nova Gorica, Vipavska 11 c, 5270 Ajdovscina, Slovenia.

- [1] K. S. Novoselov *et al.*, *Science* **306**, 666 (2004).
- [2] F. Schedin *et al.*, *Nature Mater.* **6**, 652 (2007).
- [3] A. L. Vázquez de Parga *et al.*, *Phys. Rev. Lett.* **100**, 056807 (2008).
- [4] W. Moritz *et al.*, *Phys. Rev. Lett.* **104**, 136102 (2010).
- [5] A. T. N’Diaye *et al.*, *New J. Phys.* **10**, 043033 (2008).
- [6] A. B. Preobrajenski *et al.*, *Phys. Rev. B* **78**, 073401 (2008).
- [7] T. A. Land *et al.*, *Surf. Sci.* **264**, 261 (1992).
- [8] T. Fujita *et al.*, *Surf. Interface Anal.* **37**, 120 (2005).
- [9] N. Levy *et al.*, *Science* **329**, 544 (2010).
- [10] Lahiri *et al.*, *Nature Nanotech.* **5**, 326 (2010).
- [11] B. Wang *et al.*, *New J. Phys.* **12**, 043041 (2010).
- [12] G. Giovannetti *et al.*, *Phys. Rev. Lett.* **101**, 026803 (2008).
- [13] G. Otero *et al.*, *Nature (London)* **454**, 865 (2008).
- [14] See supplementary material at <http://link.aps.org/supplemental/10.1103/PhysRevLett.105.216102> for extended experimental and theoretical details.
- [15] S. J. Clark *et al.*, *Z. Kristallogr.* **220**, 567 (2005).
- [16] J. M. Blanco *et al.*, *Prog. Surf. Sci.* **81**, 403 (2006).
- [17] P. Lacovig *et al.*, *Phys. Rev. Lett.* **103**, 166101 (2009).
- [18] W. Bao *et al.*, *Nature Nanotech.* **4**, 562 (2009).
- [19] R. Felici *et al.*, *Nature Mater.* **4**, 688 (2005).
- [20] J. Weckesser, J. V. Barth, and K. Kern, *Phys. Rev. B* **64**, 161403 (2001).
- [21] H. I. Li *et al.*, *Phys. Rev. Lett.* **103**, 056101 (2009).
- [22] X. Torrelles *et al.*, *Phys. Rev. B* **81**, 041404 (2010).
- [23] A. R. Sandy *et al.*, *Phys. Rev. Lett.* **68**, 2192 (1992).